Transaction B: Mechanical Engineering
Vol. 17, No. 5, pp. 348–357

SCIENTIA IRANICA

Contact Time Study of Electrostatically Actuated Microsystems

M. Moghimi Zand[1], B. Rashidian[2] and M.T. Ahmadian[1,*]

Abstract. *This paper presents a model to analyze contact phenomenon in microsystems actuated by ramp voltages, which has applications in frequency sweeping. First-order shear deformation theory is used to model dynamical system using finite element method, while finite difference method is applied to model squeeze film damping. The model is validated by static pull-in results. The presented hybrid FEM-FDM model is utilized to compute values of contact time and dynamic behavior. Considering this model, effects of different geometrical and mechanical parameters on contact time are studied. The influence of imposing the additional reverse voltage on dynamic characteristics of the system is also investigated. It is shown that magnitude and position of applying the reverse voltage is very important in preventing pull-in instability.*

Keywords: *Contact time; Multi-layer microplates; Pull-in instability; Squeeze film damping.*

INTRODUCTION

Electrostatic actuation is of interest for many applications. However, its nonlinear gain is an obstacle in the computational process. Electrostatically actuated microelectromechanical systems include a large group of devices such as acoustic resonators, RF switches and pressure sensors. One of the most important effects considered in designing electrostatically actuated MEMS is static pull-in instability. Static pull-in occurs by increasing the actuation voltage. If the applied voltage reaches a critical value or beyond, there will be no stable equilibrium in the system. This critical value is called the static pull-in voltage (V_{pi}) and this phenomenon is called static pull-in instability. Several investigations have been performed on pull-in instability. Osterberg has studied microstructures with circular and rectangular shapes [1]. He has achieved several closed-form models for the static pull-in phenomena in these systems and has verified these models experimentally. In another study, Abdalla et al. have considered the effect of dimensions on the static pull-in voltages of microbeams [2]. Rong et al. have presented an analytical model to study the static pull-in phenomenon of multi-layer beams using energy method [3]. Damping in microstructures is also extensively studied and reported in literature. Nayfeh and Younis have presented an approach to model squeeze film damping as an important source of extrinsic damping [4]. Younis also has modeled microstructures, considering the thermoelastic effect as an intrinsic damping [5].

When the rate of voltage variation is not negligible, the effect of inertia has to be considered. The pull-in instability related to this situation is called dynamic pull-in instability and the critical value of voltage, corresponding to the dynamic instability, is referred to as a dynamic pull-in voltage (V_{pid}) [6]. The dynamic behavior of microsystems has been investigated by several researchers. Krylov and Maimon have studied pull-in dynamics of an elastic beam actuated by electrostatic force using the Galerkin procedure to model nonlinear squeezed film damping, and rotational inertia of a mass carried by the beam [6]. Nielson and Barbastathis have performed an analysis of the dynamic characteristics of pull-in for parallel-plate and torsional electrostatic actuators using an energy-based solution for step voltages required for pull-in [7]. Rocha et al. have analyzed dynamics of the pull-in displacement for a metastable transient interval using a lumped model [8]. In some researches, effect of ambient pressure on dynamic pull-in and its applications have been studied. Nijhuis et al. have subjected the dependence of the pull-in time on ambient gas pressure [9]. In another study,

1. *Center of Excellence in Design, Robotics and Automation, School of Mechanical Engineering, Sharif University of Technology, Tehran, P.O. Box 11155-9567, Iran.*
2. *School of Electrical Engineering, Sharif University of Technology, Tehran, P.O. Box 11155-9363, Iran.*
*. *Corresponding author. E-mail: ahmadian@mech.sharif.edu*

Received 30 November 2009; accepted 16 August 2010

Gupta and Senturia have proposed a pressure sensor based on the pull-in time [10]. McCarthy et al. have used a time-transient finite difference analysis to model the dynamic behavior of two different electrostatically actuated micro switch configurations. They have used Euler-Bernoulli beam theory with considering squeeze film damping between the switch and substrate [11]. Hung and Senturia have considered a reduced-order model to investigate the behavior of electrically actuated microbeams, accounting for linear and nonlinear elastic restoring forces [12]. Dynamic behavior of electrostatically-actuated micro/nano structures have also been studied in [13-17].

Most of the studies on microstructures have been performed using step-input and harmonic actuations. However, other actuation shapes also have application in microstructures. Ramp-input actuation has applications in frequency sweeping and contact time study of RF-MEMS. Contact time is defined as the time taken by a microstructure to move from the initial position to the position where the deformable plate contacts the substrate plate.

In the present paper, contact time study of microstructures is performed. Initially, the static pull-in instability of multi- and single-layer microplates are studied. The approach utilizes First-order Shear Deformation Theory (FSDT) of multi-layer plates coupled with nonlinear electrostatic actuation and Reynolds equation. The static pull-in results have been compared with those known from literature to verify the model. Contact time variations for ramp-input voltages are also investigated. Effects of different system parameters on contact time are analyzed. Finally, effect of applying the additional reverse voltage on contact time is also considered.

FORMULATION AND SOLUTION ALGORITHM

Finite Element Model (FEM) of the Plate

In an n-layer prismatic microplate, there are one conductive and some dielectric layers (Figure 1a). A fixed planar electrode underlies the plate as a substrate. The multi-layer microplate is deformable while the substrate plate is rigid. When a voltage applied between the microplate conductive layer and the substrate plate, an attractive electrostatic force causes the microplate to deform. The length of the plate is l, the width is b, the density of the ith layer is ρ_i, the thickness of the ith layer is h_i, the plate total thickness is h, the relative permittivity of the ith layer is ε_i^r, the air permittivity is ε_0 and the air initial gap is d_{gap}. x and y are in-plane coordinates, z is the coordinate along thickness, t is the time, I_i are the mass moments of inertia ($i = 1, 2, 3$), $\varphi_x(\varphi_y)$ are the rotations of a transverse normal about y-axis (x-axis), $\hat{N}_{ij}$ are in-plane applied forces ($i, j = x, y$) and $\hat{N}_{ij}^k$ are in-plane applied forces in each layer ($k = 1, \cdots, n$) and σ_k is the stress in each layer due to $\hat{N}_{ij}^k$. Finally u_0, v_0 and w_0 are the midplane displacements along x-, y- and z-axes respectively and V is the applied voltage.

In the electrostatic actuated MEMS, the basic system is a parallel-plate capacitor. For a single-layer microplate, the capacitance formed by the part of the plate with the surface of $dx \times dy$ and the fixed substrate plate is:

$$dC_s = \frac{\varepsilon_0 dxdy}{d_{\text{gap}} - w_0(x,y)}. \tag{1}$$

Using Equation 1, in a single-layer microplate, the electrostatic force per unit area takes the following form:

$$q_{es} = -\frac{1}{2}\frac{\varepsilon_0 V^2}{(d_{\text{gap}} - w_0(x,y))^2}. \tag{2}$$

For a multi-layer microplate, the capacitance formed by the part of a multi-layer microplate with the surface of $dx \times dy$ and the ground is expressed as [3]:

$$dC_m = \frac{\varepsilon_0 dxdy}{\bar{d}_{\text{gap}} - w_0(x,y)}, \tag{3}$$

where:

$$\bar{d}_{\text{gap}} = d_{\text{gap}} + \sum_{i=1}^{n_d} h_i/\varepsilon_i^r. \tag{4}$$

$\bar{d}_{\text{gap}}$ is called the effective gap [3]. Here n_d is the

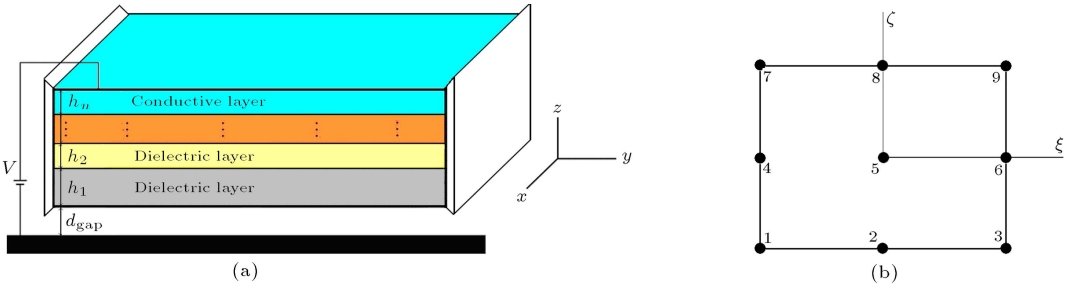

Figure 1. (a) The side view of multi-layer microplate with double-clamped boundary conditions. (b) The numbering of nodes in a nine-node element.

number of layers, which are underneath the conductive layer.

Using Equations 2 and 3 for a multi-layer microplate, the electrostatic force per unit area can be written as:

$$q_{em} = -\frac{1}{2}\frac{\varepsilon_0 V^2}{(\bar{d}_{\rm gap} - w_0(x,y))^2}. \tag{5}$$

The squeeze film damping occurs because of the massive movement of the fluid underneath the plate [5]. The effect of squeeze film damping can be modeled by compressible (nonlinear) Reynolds equation as:

$$\frac{\partial}{\partial x}\left((d_{\rm gap}-w_0)^3 P\frac{\partial P}{\partial x}\right)+\frac{\partial}{\partial y}\left((d_{\rm gap}-w_0)^3 P\frac{\partial P}{\partial y}\right) = 12\eta\left((d_{\rm gap}-w_0)\frac{\partial P}{\partial t}-P\frac{\partial w_0}{\partial t}\right), \tag{6}$$

where P and η are the total pressure and the effective viscosity of the fluid, respectively [18]. Considering Equations 5 and 6, assuming First-order Shear Deformation Theory (FSDT) and using the dynamic version of the principle of virtual displacements, one gets [19]:

$$\delta u_0 : \frac{\partial N_{xx}}{\partial x}+\frac{\partial N_{xy}}{\partial y} = I_0\frac{\partial^2 u_0}{\partial t^2}+I_1\frac{\partial^2 \phi_x}{\partial t^2},$$

$$\delta v_0 : \frac{\partial N_{xy}}{\partial x}+\frac{\partial N_{yy}}{\partial y} = I_0\frac{\partial^2 v_0}{\partial t^2}+I_1\frac{\partial^2 \phi_y}{\partial t^2},$$

$$\delta w_0 : \frac{\partial Q_x}{\partial x}+\frac{\partial Q_y}{\partial y}-\frac{1}{2}\frac{\varepsilon_0 V^2}{(\bar{d}_{\rm gap}-w_0)^2}+(P-P_0) = I_0\frac{\partial^2 w_0}{\partial t^2},$$

$$\delta \phi_x : \frac{\partial M_{xx}}{\partial x}+\frac{\partial M_{xy}}{\partial y} = I_1\frac{\partial^2 u_0}{\partial t^2}+I_2\frac{\partial^2 \phi_x}{\partial t^2},$$

$$\delta \phi_y : \frac{\partial M_{xy}}{\partial x}+\frac{\partial M_{yy}}{\partial y} = I_1\frac{\partial^2 v_0}{\partial t^2}+I_2\frac{\partial^2 \phi_y}{\partial t^2},$$

$$\frac{\partial}{\partial x}\left((d_{\rm gap}-w_0)^3 P\frac{\partial P}{\partial x}\right)+\frac{\partial}{\partial y}\left((d_{\rm gap}-w_0)^3 P\frac{\partial P}{\partial y}\right) = 12\eta\left((d_{\rm gap}-w_0)\frac{\partial P}{\partial t}-P\frac{\partial w_0}{\partial t}\right). \tag{7}$$

The structural boundary conditions for double-clamped microplates are expressed as:

$$u_0(0,y,t) = v_0(0,y,t) = w_0(0,y,t) = \varphi_x(0,y,t) = \varphi_y(0,y,t) = 0,$$
$$u_0(l,y,t) = v_0(l,y,t) = w_0(l,y,t) = \varphi_x(l,y,t) = \varphi_y(l,y,t) = 0. \tag{8}$$

The pressure boundary conditions are expressed as:

$$\frac{\partial P}{\partial x}(0,y,t) = 0, \qquad \frac{\partial P}{\partial x}(l,y,t) = 0,$$
$$P(x,0,t) = P_0, \qquad P(x,b,t) = P_0, \tag{9}$$

where N_{ij}, M_{ij}, Q_j, P, P_0 and n_d are in-plane force resultants, moment resultants, transverse force resultants, total pressure, ambient pressure and number of layers placed underneath the conductive layer respectively. N_{ij}, M_{ij} and Q_j are defined in the Appendix. Using equivalent single-layer theories to model multi-layer plates, multiplying equations of motion by δu_0, δv_0, δw_0, $\delta\varphi_x$ and $\delta\varphi_y$ and integrating by parts over the domain, results in the weakened expressions. Assuming quadratic Lagrange interpolation functions in element coordinates (ξ, η), the semi-discrete linear finite element model is obtained as [19]:

$$(\{K_e\}+\{G_e\})\{W_e\}+\{M_e\}\{\ddot{W}_e\} = \{F_e\}, \tag{10}$$

where $\{K_e\}$, $\{G_e\}$, $\{W_e\}$, $\{F_e\}$ and $\{M_e\}$ are stiffness, in-plane force, deflection, force and mass matrices, which have been presented by Reddy [19]. The electrostatic and pressure terms are involved in vector $\{F_e\}$. The finite element model of the total problem is found by assembling the equations of various elements. The numbering of nodes in the local coordinates is presented in Figure 1b. It should be noted that the numerical integration over the length of an arbitrary element is performed using Gaussian quadrature method.

Finite Difference Model (FDM) for Squeeze Film Damping

To consider the effect of squeeze film damping, Equation 6 can be rewritten as [19]:

$$(d_{\rm gap}-w_0)^3\left(\frac{\partial^2(P^2)}{\partial x^2}\right)+(d_{\rm gap}-w_0)^3\left(\frac{\partial^2(P^2)}{\partial y^2}\right) + 3(d_{\rm gap}-w_0)^2\frac{\partial}{\partial x}(d_{\rm gap}-w_0)\frac{\partial(P^2)}{\partial x} + 3(d_{\rm gap}-w_0)^2\frac{\partial}{\partial y}(d_{\rm gap}-w_0)\frac{\partial(P^2)}{\partial y} = 24\eta\left((d_{\rm gap}-w_0)\frac{\partial P}{\partial t}-P\frac{\partial w_0}{\partial t}\right). \tag{11}$$

Discretizing Equation 11 results in [19]:

$$(d_{\text{gap}}-w_{i,j}^{t})^{3}\left[\left(\frac{(P_{i+1,j}^{t})^{2}+(P_{i-1,j}^{t})^{2}-(2P_{i,j}^{t})^{2}}{\Delta x^{2}}\right)\right.$$
$$\left.+(d_{\text{gap}}-w_{i,j}^{t})^{3}\left(\frac{(P_{i,j+1}^{t})^{2}+(P_{i,j-1}^{t})^{2}-2(P_{i,j}^{t})^{2}}{\Delta y^{2}}\right)\right]$$
$$-3(d_{\text{gap}}-w_{i,j}^{t})^{2}\left(\frac{w_{i+1,j}^{t}-w_{i-1,j}^{t}}{2\Delta x}\right)$$
$$\left(\frac{(P_{i+1,j}^{t})^{2}-(P_{i-1,j}^{t})^{2}}{2\Delta x}\right)$$
$$-3(d_{\text{gap}}-w_{i,j}^{t})^{2}\left(\frac{w_{i,j+1}^{t}-w_{i,j-1}^{t}}{2\Delta y}\right)$$
$$\left(\frac{(P_{i,j+1}^{t})^{2}-(P_{i,j-1}^{t})^{2}}{2\Delta y}\right)$$
$$=24\eta\left((d_{\text{gap}}-w_{i,j}^{t})\frac{P_{i,j}^{t+1}-P_{i,j}^{t}}{\Delta t}-P_{i,j}\frac{w_{i,j}^{t+1}-w_{i,j}^{t}}{\Delta t}\right). \quad (12)$$

Therefore, using Equation 12, values of pressure in each time step for all nodes can be found as [19]:

$$P_{i,j}^{t+1}=P_{i,j}^{t}+\frac{P_{i,j}(w_{i,j}^{t+1}-w_{i,j}^{t})}{(d_{\text{gap}}-w_{i,j}^{t})}+\frac{\Delta t(d_{\text{gap}}-w_{i,j}^{t})^{2}}{24\eta_{\text{eff}}}$$
$$\left[\left(\frac{(P_{i+1,j}^{t})^{2}+(P_{i-1,j}^{t})^{2}-(2P_{i,j}^{t})^{2}}{\Delta x^{2}}\right)\right.$$
$$\left.+\left(\frac{(P_{i,j+1}^{t})^{2}+(P_{i,j-1}^{t})^{2}-2(P_{i,j}^{t})^{2}}{\Delta y^{2}}\right)\right]$$
$$-\frac{\Delta t(d_{\text{gap}}-w_{i,j}^{t})}{8\eta_{\text{eff}}}$$
$$\left[\frac{(w_{i+1,j}^{t}-w_{i-1,j}^{t})((P_{i+1,j}^{t})^{2}-(P_{i-1,j}^{t})^{2})}{4\Delta x^{2}}\right.$$
$$\left.+\frac{(w_{i,j+1}^{t}-w_{i,j-1}^{t})((P_{i,j+1}^{t})^{2}-(P_{i,j-1}^{t})^{2})}{4\Delta y^{2}}\right], \quad (13)$$

where i and j denotes the nodes in x- and y-directions, respectively. For the clamped sides of the plate, the boundary conditions of the pressure problem are zero flux, while free sides have the boundary conditions of zero dynamic pressure. Using these boundary conditions for edges and Equation 13 for internal nodes, values of pressure for all points can be obtained in each time step.

Dynamic Analysis Using Hybrid FEM-FDM Model

When the rate of voltage variation is not negligible, effect of Inertia should be considered. Therefore, Equation 10 is used to model the system dynamic behavior. The fully discretized form of the total problem is obtained using Newmark time discretization [19]. It is noteworthy that due to the nonlinearity of the problem, the direct iteration method is utilized to find deflections in each time step. The iteration process in each time step is continued until the convergence criteria of deflections are satisfied. Using deflections of the current step and deflections and pressures of the previous step, pressures of the current step can be calculated using finite difference method.

SIMULATION AND DISCUSSION

Model Validation by Static Pull-in Analysis of Multi-Layer Microplates

Calculating static pull-in voltages is essential in design process to analyze sensitivity, frequency response and dynamic range of the system [20]. Besides, this phenomenon can be utilized to validate new models. To calculate static pull-in voltages, effects of damping and inertia in Equation 10 are ignored. A computer code is utilized to calculate static pull-in voltages. This code is faster and requires less memory than commercially available finite element codes. This is due to the fact that the effect of squeeze film damping is considered by using a stable finite difference model instead of using a finite element model. Consequently, the matrices and vectors of the microplate are very smaller. In fact, one of the main advantages of using the hybrid FEM-FED model is reduction of the matrices and vectors, as discussed in [21]. Using this code, values of V_{pi} for 2-layer microplates are presented in Figures 2a and 2b [20]. In these microplates, the dielectric layers are Si_3N_4 and the conductive layers are gold. E_i and ρ_i are Young's modulus and density of each layer respectively. As seen in Figures 2a and 2b, values of static pull-in voltage (V_{pi}) are in good agreement with those reported by Rong et al. [3]. It can be concluded that the method is able to calculate static pull-in voltages of multi-layer plates correctly.

Contact Time Study of Single- and Multi-Layer Microplates

Step-Input Voltage

Using the described method in the previous sections, the diagrams of dynamic deflection versus time for various voltages can be plotted. First, consider a

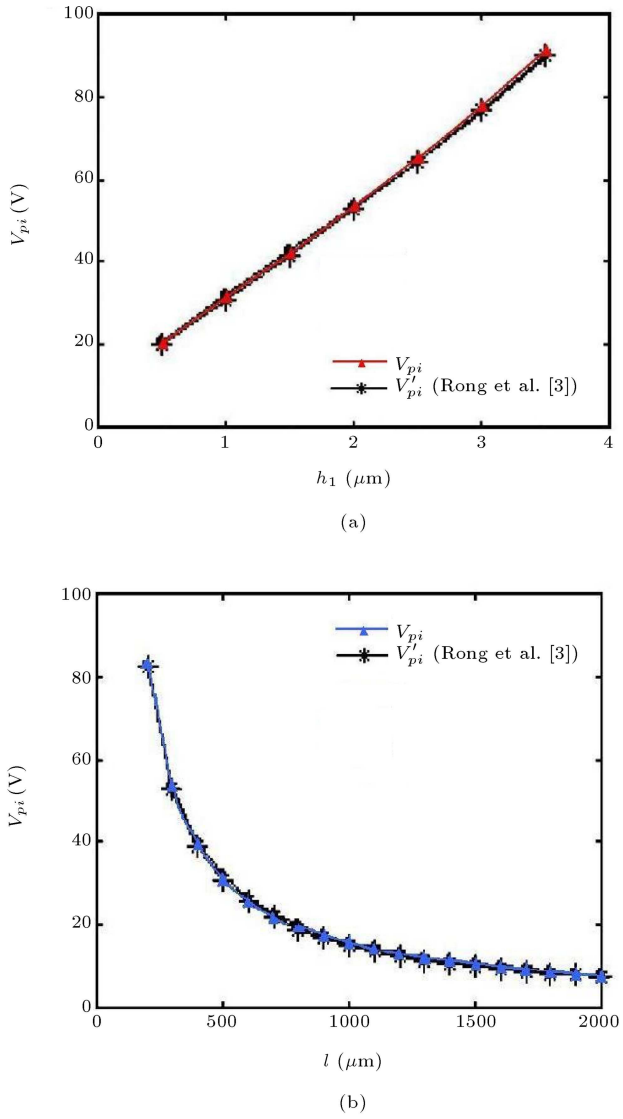

Figure 2. (a) Pull-in voltage versus thickness of Si_3N_4 layer [20]; $l = 500$ μm, $b = 50$ μm, $h_2 = 0.5$ μm, $d_{\text{gap}} = 1$ μm, $E_1 = 250$ GPa, $E_2 = 53$ GPa, $\sigma_1 = 500$ MPa, $\sigma_2 = 12$ MPa, $\varepsilon_1^r = 8$. (b) Pull-in voltage versus length of the plate [20]; $b = 50$ μm, $h_1 = 1$ μm, $h_2 = 0.5$ μm, $d_{\text{gap}} = 1$ μm, $E_1 = 250$ GPa, $E_2 = 53$ GPa, $\sigma_1 = 500$ MPa, $\sigma_2 = 12$ MPa and $\varepsilon_1^r = 8$.

microplate actuated by a step-input voltage. In Figure 3, diagram of contact time versus voltage for various ambient pressures is shown. The double-clamped microplate consists of two layers: The upper layer is gold and the bottom layer is Si_3N_4. Note that the actuation voltages are all beyond the dynamic pull-in voltage (undamped $V_{pid} = 78.1$ V). Figure 3 shows that for a constant ambient pressure, an increase in the actuation voltage leads to a decrease in the contact time. Another parameter, which influences contact time, is the ambient pressure. As seen in Figure 3, increasing the ambient pressure, results in increasing the contact time.

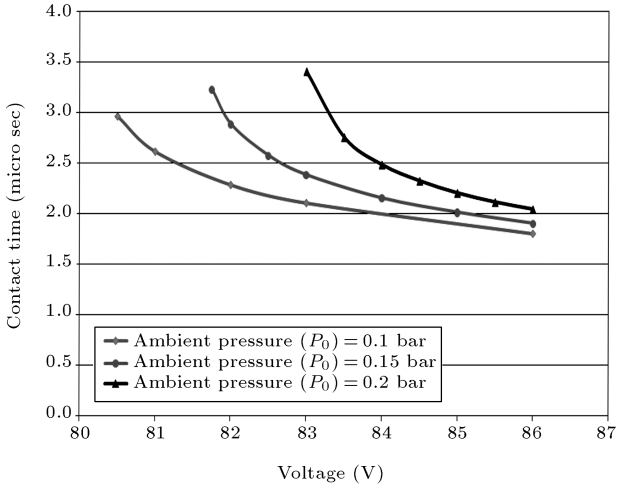

Figure 3. Contact time versus forward voltage for a multi-layer microplate with ramp voltage actuation. $b = 50$ μm, $h_1 = 3$ μm, $h_2 = 0.5$ μm, $d_{\text{gap}} = 1$ μm, $E_1 = 250$ GPa, $E_2 = 53$ GPa, $\sigma_1 = 0$, $\sigma_2 = 0$, $\varepsilon_1^r = 8$, $\rho_1 = 3100$ kg/m^3, $\rho_2 = 19300$ kg/m^3, $V_{\text{pid}} = 78.1$ Volt (undamped).

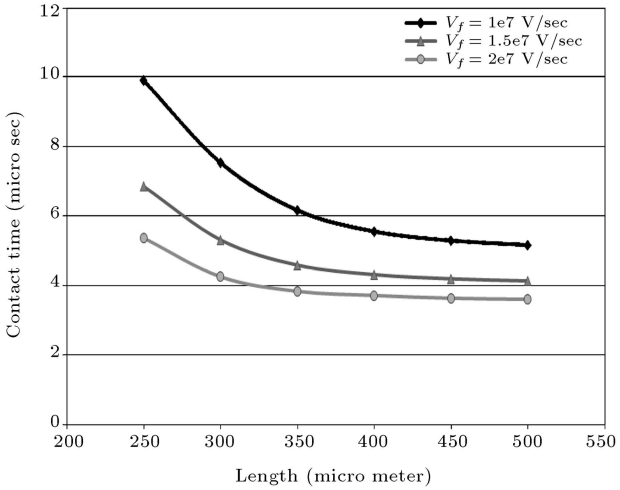

Figure 4. Contact time versus length of the plate for single-layer microplates with different rate of voltage variation actuated by ramp voltage. $b = 50$ μm, $h_1 = 3$ μm, $h_2 = 0.5$ μm, $d_{\text{gap}} = 1$ μm, $E_1 = 250$ GPa, $E_2 = 53$ GPa, $\sigma_1 = 0$, $\sigma_2 = 0$, $\varepsilon_1^r = 8$, $\rho_1 = 3100$ kg/m^3, $\rho_2 = 19300$ kg/m^3, $P_0 = 0$ bar (undamped system).

Ramp-Input Voltage

Now, let us consider microplates actuated by ramp-input voltages. In Figure 4, diagram of contact time versus length for various values of voltage rate is shown. As it can be seen in this figure, for a constant voltage rate (V_f), by increasing the length of the plate, the contact time decreases. Such behavior is reasonable because longer plates have less stiffness. Nevertheless, increasing the width of the plates causes no significant variations in contact time. It is also useful to consider the variations of contact Time versus

voltage rate. This diagram is depicted in Figure 5 for two plate lengths. Interestingly, the curves for different lengths converge to each other by increasing the voltage rate.

In Figure 6, diagram of contact time versus d_{gap} for various values of voltage rate is shown. This diagram is depicted for a single-layer double-clamped plate, actuated by a ramp voltage. It can be seen that for a constant voltage rate, by increasing the air gap, contact time increases due to a decrease in the electrostatic force, and by increasing the rate of voltage results in decreasing the contact time.

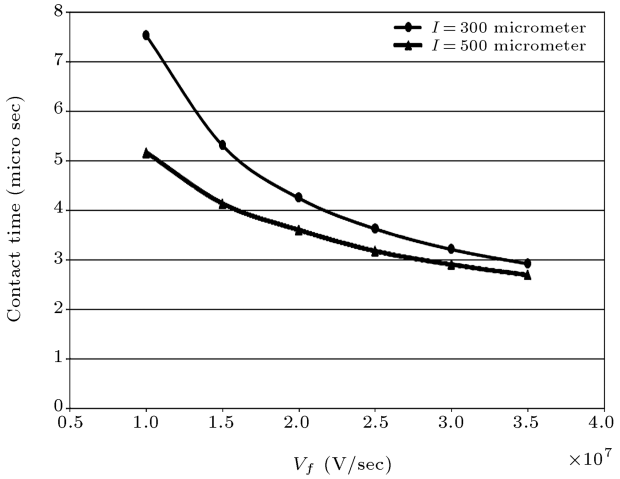

Figure 5. Contact time versus rate of voltage variation for single-layer microplates with ramp voltage actuation and two different lengths. $b = 50$ μm, $h_1 = 3$ μm, $h_2 = 0.5$ μm, $d_{\text{gap}} = 1$ μm, $E_1 = 250$ GPa, $E_2 = 53$ GPa, $\sigma_1 = 0$, $\sigma_2 = 0$, $\varepsilon_1^r = 8$, $\rho_1 = 3100$ kg/m^3, $\rho_2 = 19300$ kg/m^3, $P_0 = 0$ bar (undamped system).

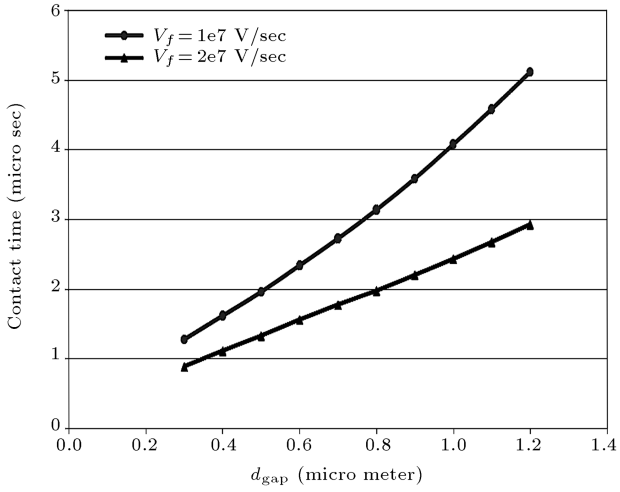

Figure 6. Contact time versus air gap for single-layer microplates with ramp voltage actuation and two different rate of voltage variation. $l = 250$ μm, $b = 50$ μm, $h_1 = 2.5$ μm, $d_{\text{gap}} = 1$ μm, $E_1 = 149$ GPa, $\sigma_1 = 0$, $\varepsilon_1^r = 8$, $\rho_1 = 2330$ kg/m^3, $P_0 = 0$ bar (undamped system).

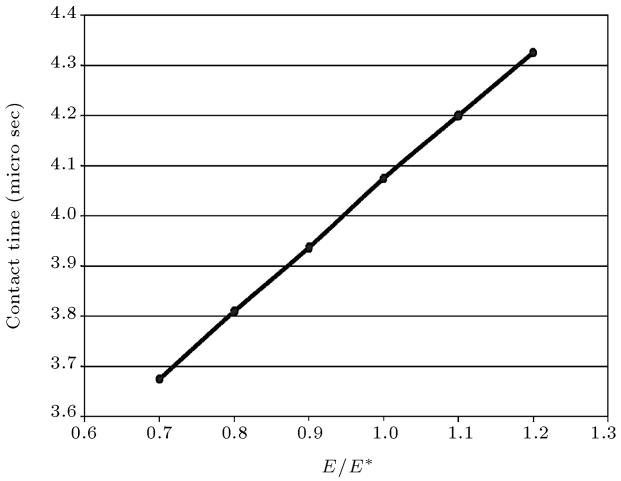

Figure 7. Contact time versus elastic modulus for single-layer microplates actuated by ramp-input voltage. $l = 250$ μm, $b = 50$ μm, $h_1 = 2.5$ μm, $d_{\text{gap}} = 1$ μm, $E^* = 149$ GPa, $\sigma_1 = 0$, $\varepsilon_1^r = 8$, $\rho_1 = 2330$ kg/m^3, $P_0 = 0$ bar (undamped system).

Elastic modulus is another characteristic which has an important effect on the behavior of microplates. In Figure 7, diagram of contact time versus normalized elastic modulus for a single-layer microplate is illustrated. It was predictable that due to the linear relationship between plate stiffness and elastic modulus of the plate, there is a linear relationship between contact time and elastic modulus of the plate. This is also true for a multi-layer microplate, considering the equivalent elastic modulus, instead of elastic modulus of each layer.

In addition to the mechanical and geometrical properties, dynamic behavior of microplates depends on the type of input voltage. For the ramp-input voltage, the ratio of voltage rate over d_{gap} is an important parameter. In Figure 8, a comparison is performed between two cases with equal ratio of voltage rate over d_{gap}: one of them with the air gap of 0.6 μm and the voltage rate of 10 MV/sec and the other with the air gap of 1.2 μm and the voltage rate of 20 MV/sec. In Figure 8a, the midpoint deflection versus time is depicted, while in Figure 8b, normalized deflection versus normalized time is illustrated. For normalizing deflection and time, air gap (d_{gap}) and contact time (T_{contact}) are used, respectively. It can be concluded from these figures that microplates with equal ratio of voltage rate over air gap show similar behavior. In Figure 8a, it is clear that the curve under the contact point for microsystem with the air gap of 0.6 μm does not have any physical meaning.

Reverse Ramp-Input Voltage

By applying a constant forward ramp voltage (V_f), the occurrence of contact is inevitable. In order to avoid

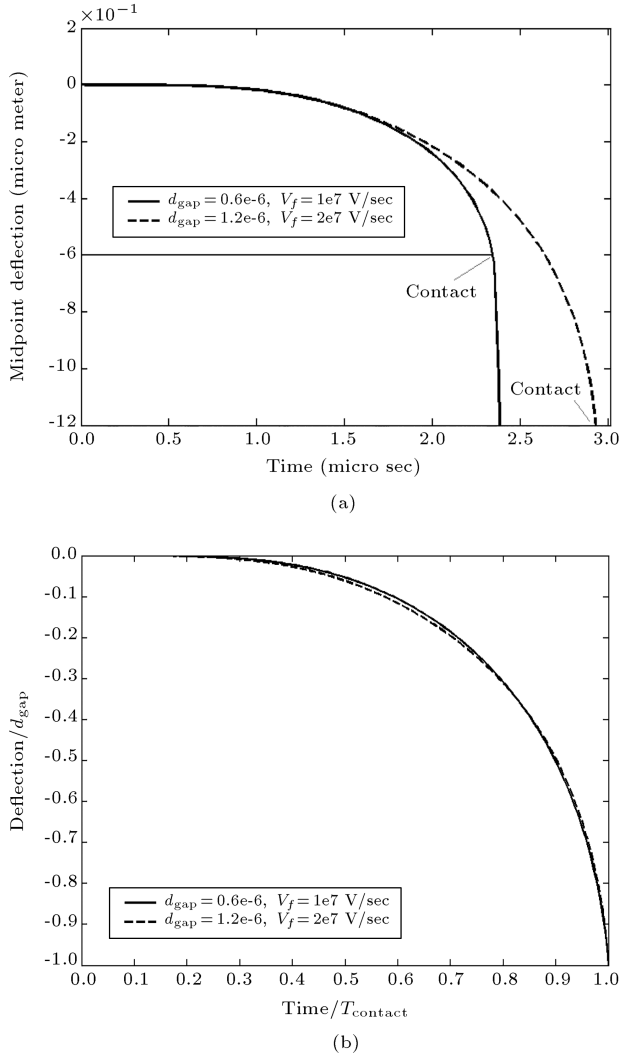

Figure 8. (a) Deflection versus time. (b) Normalized deflection versus normalized time for single-layer microplates with ramp voltage actuation. $b = 50$ μm, $h_1 = 3$ μm, $h_2 = 0.5$ μm, $d_{\text{gap}} = 1$ μm, $E_1 = 250$ GPa, $E_2 = 53$ GPa, $\sigma_1 = 0$, $\sigma_2 = 0$, $\varepsilon_1^r = 8$, $\rho_1 = 3100$ kg/m^3, $\rho_2 = 19300$ kg/m^3, $P_0 = 0$ bar (undamped system).

the contact, a reverse ramp voltage (V_r) can be applied. The reverse ramp voltage is applied when the midpoint deflection is d_r. The magnitude of the reverse voltage and the position at which the reverse voltage is applied is very important in avoiding contact. As an example, for a 2-layer microplate, diagram of deflection and voltage versus time is presented in Figure 9. As seen in this figure, the reverse ramp voltage is applied when the midpoint deflection reaches 0.5 d_{gap} (i.e. $d_r = 0.5$ d_{gap}).

In Figure 10, diagram of contact time versus rate of reverse voltage is presented. In this analysis, the reverse voltage is applied when midpoint reaches 0.5 d_{gap} (i.e. $d_r = 0.5$ d_{gap}). From the figure, it should be noted that increasing the rate of reverse voltage results in increasing the slope of the curve.

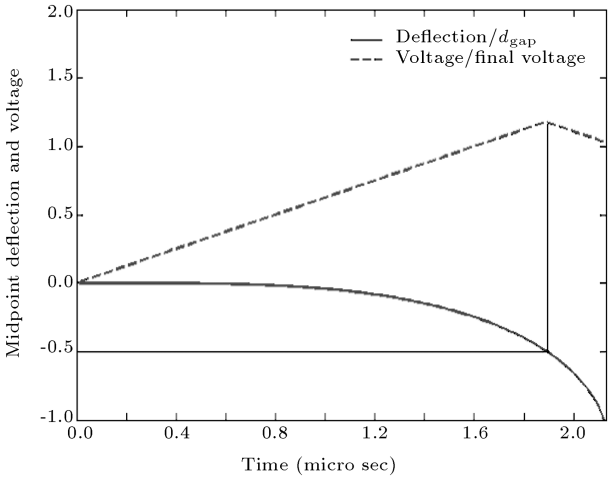

Figure 9. Deflection versus time and voltage versus time. $l = 250$ μm, $b = 50$ μm, $h_1 = 2.5$ μm, $d_{\text{gap}} = 1$ μm, $E^* = 149$ GPa, $\sigma_1 = 0$, $\rho_1 = 2330$ kg/m^3, $V_f = 25$ MV/sec, $V_r = 25$ MV/sec and $P_0 = 0$ bar (undamped system).

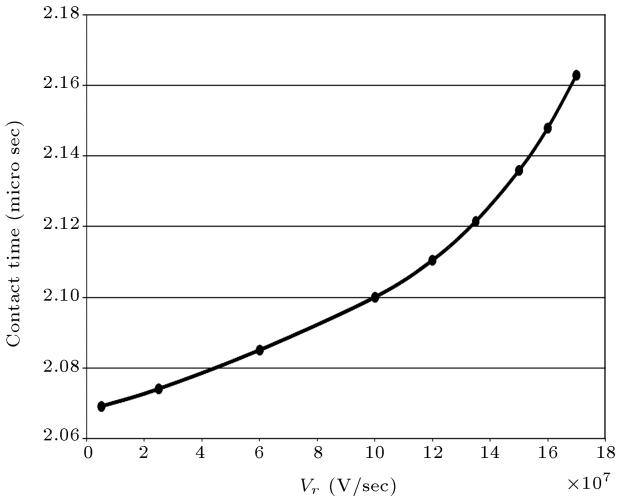

Figure 10. Contact time versus rate of reverse voltage for single-layer microplates actuated by ramp input voltage. $l = 250$ μm, $b = 50$ μm, $h_1 = 2.5$ μm, $d_{\text{gap}} = 1$ μm, $E^* = 149$ GPa, $\sigma_1 = 0$, $\rho_1 = 2330$ kg/m^3, $V_f = 25$ MV/sec, $d_r = 0.5$ d_{gap}, $P_0 = 0$ bar (undamped system).

The contact time approaches infinity for large rate of reverse voltage, which means that contact between plates can be prevented in the system. In Figure 11, diagram of contact time versus d_r is depicted. As seen by decreasing d_r (i.e. the position at which the reverse voltage is imposed), the contact time increases monotonically.

It should be noted that when reverse voltage is imposed later in time (i.e. the deformable plate is closer to the substrate), preventing the contact is more complicated and applying reverse voltages with higher rates are required. Considering the limitations of the

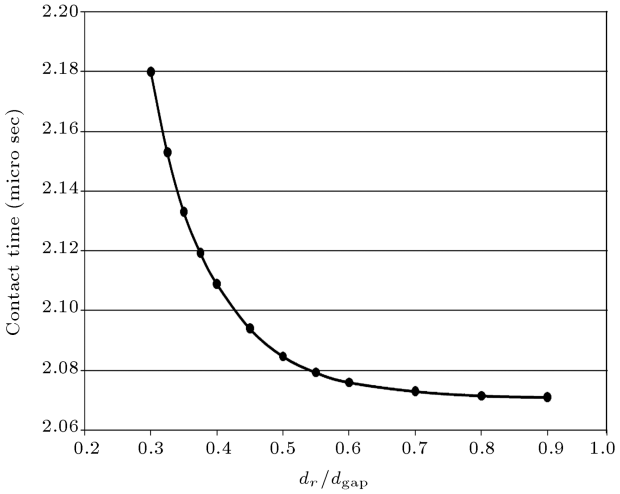

Figure 11. Contact time versus position of imposing reverse voltage for single-layer microplates actuated by ramp input voltage. $l = 250$ μm, $b = 50$ μm, $h_1 = 2.5$ μm, $d_{\text{gap}} = 1$ μm, $E^* = 149$ GPa, $\sigma_1 = 0$, $\rho_1 = 2330$ kg/m^3, $V_f = 25$ MV/sec, $V_r = 25$ MV/sec and $P_0 = 0$ bar (undamped system).

physical system, the rate of reverse voltage cannot be increased without any restriction. Therefore, for a constant rate of forward voltage, when the position of imposing the reverse voltage (d_r) exceeds some critical value, occurrence of contact is inevitable. In other words, occurrence of the contact is not preventable by imposing reverse voltage from every position, even by applying maximum feasible magnitude of the reverse voltage.

CONCLUSION

Dynamic behavior of microstructures subjected to electric field has been investigated. The hybrid FEM-FDM model has been developed to consider in-plane forces, nonlinear electrostatic actuation and nonlinear squeeze film damping using first-order shear deformation theory. Static pull-in analysis of multi-layer microplates has been performed and results are in good agreement with literature. Dynamic behavior has been analyzed to study the contact between the microplate and substrate. Using the model, effects of different geometrical and mechanical parameters of the system have been studied. It has been shown that increasing the ambient pressure and elastic modulus, increases the contact time, while increasing the length and voltage rate, decreases it. Finally, the influence of applying reverse ramp voltage on the microplate dynamic characteristics has been considered. It can be concluded that preventing the contact by applying the reverse voltage is not feasible in all positions. This model will be useful in designing coupled-domain multi-layer microplates with applications in frequency sweeping.

REFERENCES

1. Osterberg, P.M. "Electrostatically actuated microelectromechanical test structures for material property measurement", PhD dissertation, Massachusetts Institute of Technology (1995).
2. Abdalla, M.M., Reddy, C.K., Faris, W.F. and Gurdal, Z. "Optimal design of an electrostatically actuated microbeam for maximum pull-in voltage", *Computers and Structures*, **83**, pp. 1320-1329 (2005).
3. Rong, H., Huang, Q.A., Nie, M. and Li, W. "An analytical model for pull-in voltage of double-clamped multilayer beams", *Sensors and Actuators A*, **116**, pp. 15-21 (2004).
4. Nayfeh, A.H. and Younis, M.I. "A new approach to the modeling and simulation of flexible microstructures under the effect of squeeze film damping", *J. Micromech. Microeng*, **14**, pp. 170-181 (2004).
5. Younis, M.I. "Modeling and simulation of microelectromechanical systems in multi-physics fields", PhD dissertation, Virginia Polytechnic Institute and state University (2004).
6. Krylov, S. and Maimon, R. "Pull-in dynamics of an elastic beam actuated by continuously distributed electrostatic force", *ASME Journal of Vibration and Acoustics*, **126**(3), pp. 332-342 (2004).
7. Nielson, G.N. and Barbastathis, G. "Dynamic pull-in of parallel-plate and torsional electrostatic MEMS actuators", *J. of Microelectrimechanical Systems*, **15**(4), pp. 811-821 (2006).
8. Rocha, L.A., Cretu, E. and Wolffenbuttel, R.F. "Behavioural analysis of the pull-in dynamic transition", *J. Micromech. Microeng.*, **14** (2004).
9. Nijhuis, M.H.H., Basten, T.G.H., Wijnant, Y.H., Tijdeman, H. and Tilmans, H.A.C. "Transient non-linear response of 'pull-in MEMS devices' including squeeze film effects", *Proc. Eurosensors* XIII, The Hague, The Netherlands, pp. 729-732 (1999).
10. Gupta, R.K. and Senturia, S.D. "Pull-in time as a measure of absolute pressure", *Proc. MEMS'97*, Nagoya, Japan, pp. 290-294 (1997).
11. McCarthy, B., Adams, G.G. McGruer, N.E., and Potter, D. "A dynamic model, including contact bounce, of an electrostatically actuated microswitch", *IEEE Journal of Microelectromechanical Systems*, **11**(3), pp. 276-283 (2002).
12. Hung, E.S. and Senturia, S.D. "Generating efficient dynamical models for microelectromechanical systems from a few finite-element simulation runs", *IEEE Journal of Microelectomechanical Systems*, **8**(3), pp. 280-289 (1999).
13. Moghimi Zand, M., Ahmadian, M.T. and Rashidian, B. "Semi-analytic solutions for nonlinear vibrations of microbeams under suddenly applied voltages", *Journal of Sound and Vibration*, **325**(1-2), pp. 382-396 (7 Aug. 2009).

14. Moghimi Zand, M. and Ahmadian, M.T. "Application of homotopy analysis method in studying dynamic pull-in instability of microsystems", *Mechanics Research Communications*, **36**(7), pp. 851-858 (Oct. 2009).

15. Tajalli, S.A., Moghimi Zand, M. and Ahmadian, M.T. "Effect of geometric nonlinearity on dynamic pull-in behavior of coupled-domain microsystems based on classical and shear deformation plate theories", *European Journal of Mechanics - A/Solids*, **28**(5), pp. 916-925 (Sept.-Oct. 2009).

16. Moghimi Zand, M. and Ahmadian, M.T. "Vibrational analysis of electrostatically actuated microstructures considering nonlinear effects", *Communications in Nonlinear Science and Numerical Simulations*, **14**(4), pp. 1664-1678 (2009).

17. Moghimi Zand, M. and Ahmadian, M.T. "Dynamic pull-in instability of electrostatically actuated beams incorporating Casimir and van der Waals forces", *Proceedings of the Institution of Mechanical Engineers, Part C, Journal of Mechanical Engineering Science* (In press).

18. Veijola, T., Kuisma, H., Lahdenpera, J. and Ryhanen, T. "Equivalent-circuit model of the squeezed gas film in a silicon accelerometer", *Journal of Sensors and Actuators*, **A48**, pp. 235-248 (1995).

19. Reddy, J.N., *Mechanics of Laminated Composite Plates and Shells: Theory and Analysis* (2004).

20. Moghimi Zand, M. and Ahmadian, M.T. "Characterization of coupled-domain multi-layer microplates in pull-in, vibrations and transient behavior", *International Journal of Mechanical Sciences*, **49**(11), pp. 1226-1237 (2007).

21. Santis, V.D., Feliziani, M. and Maradei, F. "Hybrid finite element/finite difference (FE/FD) model to analyze thermal transients in biological vascularized tissues", *The International Journal for Computation and Mathematics in Electrical and Electronic Engineering*, **27**(6), pp. 1307-1318 (2008).

APPENDIX

Force-Displacement Relations

In each layer, the stress-strain relations in the laminate coordinates can be written as [19]:

$$\begin{Bmatrix}\sigma_{xx}\\ \sigma_{yy}\\ \sigma_{xy}\end{Bmatrix} = \begin{bmatrix}\overline{Q}_{11} & \overline{Q}_{12} & \overline{Q}_{16}\\ \overline{Q}_{12} & \overline{Q}_{22} & \overline{Q}_{26}\\ \overline{Q}_{16} & \overline{Q}_{26} & \overline{Q}_{66}\end{bmatrix} \begin{Bmatrix}\varepsilon_{xx}\\ \varepsilon_{yy}\\ \varepsilon_{xy}\end{Bmatrix},$$

$$\begin{Bmatrix}\sigma_{yz}\\ \sigma_{xz}\end{Bmatrix} = \begin{bmatrix}\overline{Q}_{44} & \overline{Q}_{45}\\ \overline{Q}_{45} & \overline{Q}_{55}\end{bmatrix} \begin{Bmatrix}\varepsilon_{yz}\\ \varepsilon_{xz}\end{Bmatrix}. \tag{A1}$$

Using Equivalent Single-Layer (ESL) theories and by integrating Equation A1 over the plate thickness, one obtains [19]:

$$\begin{Bmatrix}N_{xx}\\ N_{yy}\\ N_{xy}\end{Bmatrix} = \int_{z=-\frac{h}{2}}^{z=\frac{h}{2}} \begin{Bmatrix}\sigma_{xx}\\ \sigma_{yy}\\ \sigma_{xy}\end{Bmatrix} dz,$$

$$\begin{Bmatrix}M_{xx}\\ M_{yy}\\ M_{xy}\end{Bmatrix} = \int_{z=-\frac{h}{2}}^{z=\frac{h}{2}} \begin{Bmatrix}\sigma_{xx}\\ \sigma_{yy}\\ \sigma_{xy}\end{Bmatrix} z dz,$$

$$\begin{Bmatrix}Q_x\\ Q_y\end{Bmatrix} = K \int_{z=-\frac{h}{2}}^{z=\frac{h}{2}} \begin{Bmatrix}\sigma_{xz}\\ \sigma_{yz}\end{Bmatrix} dz, \tag{A2}$$

where N_{ij}, M_{ij} and Q_i are in-plane force resultants, moment resultants and transverse force resultants, respectively. By replacing the values of stresses in Equation A2, one gets [19]:

$$\begin{Bmatrix}N_{xx}\\ N_{yy}\\ N_{xy}\end{Bmatrix} = \begin{bmatrix}A_{11} & A_{12} & A_{16}\\ A_{12} & A_{22} & A_{26}\\ A_{16} & A_{26} & A_{66}\end{bmatrix} \begin{Bmatrix}\frac{\partial u_0}{\partial x} + \frac{1}{2}\left(\frac{\partial w_0}{\partial x}\right)^2\\ \frac{\partial v_0}{\partial y} + \frac{1}{2}\left(\frac{\partial w_0}{\partial y}\right)^2\\ \frac{\partial u_0}{\partial y} + \frac{\partial v_0}{\partial x} + \frac{\partial w_0}{\partial x}\frac{\partial w_0}{\partial y}\end{Bmatrix} + \begin{bmatrix}B_{11} & B_{12} & B_{16}\\ B_{12} & B_{22} & B_{26}\\ B_{16} & B_{26} & B_{66}\end{bmatrix} \begin{Bmatrix}\frac{\partial \varphi_x}{\partial x}\\ \frac{\partial \varphi_y}{\partial y}\\ \frac{\partial \varphi_x}{\partial y} + \frac{\partial \varphi_y}{\partial x}\end{Bmatrix}, \tag{A3}$$

$$\begin{Bmatrix}M_{xx}\\ M_{yy}\\ M_{xy}\end{Bmatrix} = \begin{bmatrix}B_{11} & B_{12} & B_{16}\\ B_{12} & B_{22} & B_{26}\\ B_{16} & B_{26} & B_{66}\end{bmatrix} \begin{Bmatrix}\frac{\partial u_0}{\partial x} + \frac{1}{2}\left(\frac{\partial w_0}{\partial x}\right)^2\\ \frac{\partial v_0}{\partial y} + \frac{1}{2}\left(\frac{\partial w_0}{\partial y}\right)^2\\ \frac{\partial u_0}{\partial y} + \frac{\partial v_0}{\partial x} + \frac{\partial w_0}{\partial x}\frac{\partial w_0}{\partial y}\end{Bmatrix} + \begin{bmatrix}D_{11} & D_{12} & D_{16}\\ D_{12} & D_{22} & D_{26}\\ D_{16} & D_{26} & D_{66}\end{bmatrix} \begin{Bmatrix}\frac{\partial \varphi_x}{\partial x}\\ \frac{\partial \varphi_y}{\partial y}\\ \frac{\partial \varphi_x}{\partial y} + \frac{\partial \varphi_y}{\partial x}\end{Bmatrix}, \tag{A4}$$

$$\begin{Bmatrix}Q_y\\ Q_x\end{Bmatrix} = K \begin{bmatrix}A_{44} & A_{45}\\ A_{45} & A_{55}\end{bmatrix} \begin{Bmatrix}\frac{\partial w_0}{\partial y} + \varphi_y\\ \frac{\partial w_0}{\partial x} + \varphi_x\end{Bmatrix}, \tag{A5}$$

where:

$$\begin{pmatrix}A_{ij} & B_{ij} & D_{ij}\end{pmatrix} = \int_{-\frac{h}{2}}^{\frac{h}{2}} \bar{Q}_{ij} \begin{pmatrix}1 & z & z^2\end{pmatrix} dz, \tag{A6}$$

here K is the shear correction coefficient.

BIOGRAPHIES

Mahdi Moghimi Zand received his BS (with the highest honor) in Mechanical Engineering from Isfahan University of Technology in 2004. He also received his MS and PhD (with the highest honor) in Mechanical Engineering from Sharif University of Technology in 2005 and 2008, respectively. He has won a number of academic awards and scholarships including the PhD fellowship of the Iranian National Elite Foundation. His active fields of research are Nonlinear Vibrations, Computational Mechanics and MEMS.

Bizhan Rashidian received his B.S. and M.S. (with the highest honor), both in Electrical Engineering, from University of Tehran in 1986 and 1988, respectively.

He received his Ph.D. in 1993 from Georgia Institute of Technology. He has been a Professor at the School of Electrical Engineering, Sharif University of Technology since 2003 where he joined in 1993 as assistant professor.

His active fields of research are Nanophotonics, Nanoelectronics, and MEMS.

Mohammad Taghi Ahmadian Graduated from University of Kansas with a Ph.D. degree in physics in 1980, and Ph.D. degree in Mechanical Engineering in 1986. He served as assistant professor in the University of Missouri and University of Kansas from 1985-1988.

Professor Ahmadian has been a member of the faculty in the School of Mechanical Engineering at Sharif University since 1989.